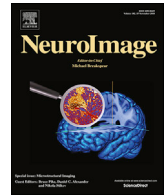




Contents lists available at ScienceDirect

NeuroImage

journal homepage: [www.elsevier.com/locate/neuroimage](http://www.elsevier.com/locate/neuroimage)

# Evaluating g-ratio weighted changes in the corpus callosum as a function of age and sex



Shai Berman<sup>a</sup>, Kathryn L. West<sup>b,c</sup>, Mark D. Does<sup>b,c</sup>, Jason D. Yeatman<sup>d</sup>, Aviv A. Mezer<sup>a,\*</sup>

<sup>a</sup> The Edmond and Lily Safra Center for Brain Sciences, The Hebrew University of Jerusalem, Jerusalem, Israel

<sup>b</sup> Department of Biomedical Engineering, Vanderbilt University, Nashville, TN, USA

<sup>c</sup> Vanderbilt University Institute of Imaging Science, Vanderbilt University, Nashville, TN, USA

<sup>d</sup> Institute for Learning & Brain Sciences and Department of Speech & Hearing Sciences, University of Washington, Seattle, WA, USA

## ARTICLE INFO

### Keywords:

g-ratio  
Corpus callosum  
Age  
Sex

## ABSTRACT

Recent years have seen a growing interest in relating MRI measurements to the structural-biophysical properties of white matter fibers. The fiber g-ratio, defined as the ratio between the inner and outer radii of the axon myelin sheath, is an important structural property of white matter, affecting signal conduction. Recently proposed modeling methods that use a combination of quantitative-MRI signals, enable a measurement of the fiber g-ratio in vivo. Here we use an MRI-based g-ratio estimation to observe the variance of the g-ratio within the corpus callosum, and evaluate sex and age related differences.

To estimate the g-ratio we used a model (Stikov et al., 2011; Duval et al., 2017) based on two different WM microstructure parameters: the relative amounts of myelin (myelin volume fraction, MVF) and fibers (fiber volume fraction, FVF) in a voxel. We derived the FVF from the fractional anisotropy (FA), and estimated the MVF by using the lipid and macromolecular tissue volume (MTV), calculated from the proton density (Mezer et al., 2013). In comparison to other methods of estimating the MVF, MTV represents a stable parameter with a straightforward route of acquisition. To establish our model, we first compared histological MVF measurements (West et al., 2016) with the MRI derived MTV. We then implemented our model on a large database of 92 subjects (44 males), aged 7 to 81, in order to evaluate age and sex related changes within the corpus callosum.

Our results show that the MTV provides a good estimation of MVF for calculating g-ratio, and produced values from the corpus callosum that correspond to those found in animals ex vivo and are close to the theoretical optimum, as well as to published in vivo data. Our results demonstrate that the MTV derived g-ratio provides a simple and reliable in vivo g-ratio-weighted (GR\*) measurement in humans. In agreement with theoretical predictions, and unlike other tissue parameters measured with MRI, the g-ratio estimations were found to be relatively stable with age, and we found no support for a significant sexual dimorphism with age.

## 1. Introduction

The study of human white matter has progressed tremendously in recent years. It is now broadly accepted that the microstructural properties of white matter change over the course of normal development (Bowley et al., 2010; Callaghan et al., 2014; Nagy et al., 2004; Yeatman et al., 2014), and correlate with cognitive functions (Moeller et al., 2015; Voineskos et al., 2012; Yeatman et al., 2011; Yeatman et al., 2012; Zatorre et al., 2012), and neuropathological states (Compston and Coles, 2008; Fields, 2008). Many of these findings were made possible by advancements in vivo magnetic resonance imaging (MRI) techniques, including quantitative MRI (qMRI), and in particular diffusion MRI

(dMRI). Recent years have seen a growing interest in relating MRI measured parameters to the structure and biophysical properties of the fibers in white matter. A recent proposal suggests that a fundamental property of the white matter, the fiber g-ratio, can be modeled by combining dMRI and other myelin sensitive qMRI signals (Dean et al., 2016; Mohammadi et al., 2015; Stikov et al., 2011, 2015a; West et al., 2015).

The fiber g-ratio is defined as the ratio of the inner to outer radius of the myelin sheath wrapped around the axon. It has been analytically shown that the g-ratio affects the signal conduction velocity of the axons (Rushon, 1951), as well their energy consumption and conduction fidelity (Chomiak and Hu, 2009). Theoretical work has concluded that the

\* Corresponding author.

E-mail address: [aviv.mezer@elsc.huji.ac.il](mailto:aviv.mezer@elsc.huji.ac.il) (A.A. Mezer).

optimal g-ratio is between 0.6 and 0.75. These studies, together with suggested coupling of axonal growth and myelination (de Waegh et al., 1992; Friede, 1972; Griffiths et al., 1998; Nave, 2010), have encouraged the assumption that the average g-ratio is fairly constant across the central nervous system (CNS) although, until very recently, this had not been tested in vivo in the human brain.

Studies that measure the g-ratio ex vivo in the CNS typically use electron microscopy (EM), and focus on either the corpus callosum or the optic nerve, where the axon bundles are clearly separated from their environment and their direction is known. The g-ratio values reported are around 0.67 for monkeys (Stikov et al., 2015a,b), 0.81 for guinea pigs (Guy et al., 1989), and 0.76 for mice (Arnett et al., 2001). These values are congruent with the optimal g-ratio values suggested by theoreticians (Chomiak and Hu, 2009; Rushton, 1951).

Claims for the significance of the g-ratio in white matter functionality highlight possible effects on cognitive functions and behavior (Paus and Toro, 2009), and may be related to abnormalities in subjects suffering from demyelinating diseases such as multiple sclerosis (Albert et al., 2007; Hampton et al., 2012; Wolswijk, 2002). Furthermore, it was suggested that the g-ratio changes during development in a sexually dimorphic fashion (Paus, 2010; Paus and Toro, 2009). Ex vivo measurements of the g-ratio show sex differences in the splenium of young rats (Pesaresi et al., 2015), however, it is still unclear whether these differences are also present in humans and whether the effect seen in rats reflects a measurable difference that can be detected in vivo.

Recent in vivo studies measured changes in the g-ratio as a function of age. Dean et al. reported a decrease in the g-ratio during early development, between 3 months and 7.5 years of age (Dean et al., 2016). Cercignani et al. measured the g-ratio of aging subjects, ages 20–80, and found an increase that was similar between males and females (Cercignani et al., 2017). Interestingly, this aging effect is in contrast with recent results in rodents that show decrease in g-ratio in the optic nerve in aging mice (Stahon et al., 2016).

A variety of qMRI approaches have been proposed to model the g-ratio based on in vivo measurements and a number of research groups (Dean et al., 2016; Mohammadi et al., 2015; Stikov et al., 2015a; West et al., 2016) have proposed methods for estimating the g-ratio by using different MRI acquisitions. These methods utilize advanced dMRI techniques to model the voxel-wise axon volume fraction (AVF), or the volume fraction of a voxel that contains fibers (axons and myelin) (also called fiber volume fraction (FVF)). Techniques used include AxCaliber (Assaf and Blumenfeld-Katzir, 2008), NODDI (Stikov et al., 2015a; Zhang et al., 2012), ActiveAx (Alexander et al., 2010; Duval et al., 2017), TFD (Mohammadi et al., 2015; Reisert et al., 2013; Ellerbrock and Mohammadi, 2016), and tensor modeling (Campbell et al., 2017; Stikov et al., 2011). The dMRI models can then be combined with other qMRI models that measure the myelin volume fraction (MVF), which refers to the volume within a voxel that is occupied by myelin sheaths. MVF estimates are not experimentally straightforward and include parameters of quantitative magnetization transfer (qMT) (Helms et al., 2008; Mohammadi et al., 2015; Sled and Pike, 2001; Stikov et al., 2015a; West et al., 2016; Yarnykh, 2007), which require scaling in order to achieve the MVF values (Campbell et al., 2017; Cercignani et al., 2017; Stikov et al., 2015a; West et al., 2016). Another potentially useful parameter is the myelin water fraction (MWF) (Mackay et al., 1994; Meyers et al., 2017; West et al., 2016). MWF is specific to myelin, but requires extended data acquisition and analysis that is rarely practical in humans (but could be of potential use in the future). Alternatively, MWF can be estimated with a faster acquisition that relies on additional modeling assumptions (Deoni et al., 2013; Deoni et al., 2008).

Recently, Duval et al. (2017) suggested the use of the lipid and macromolecular tissue volume (MTV), derived from proton density (PD) as an estimate for MVF, when measuring the g-ratio in the spinal cord. While MTV may be less specific for myelin than some alternatives (qMT, MWF), these three measurements are correlated with each other (Dula et al., 2010; Mezer et al., 2013; West et al., 2016). This correlation is higher

than the qMT scan-rescan reliability as measured in Stikov et al. (2011), and it was recently shown that PD is highly correlated with histologically measured MVF (West et al., 2016). Furthermore, the calculation of g-ratio with MTV as an estimate for MVF is comparable with other calculations (Ellerbrock and Mohammadi, 2016). Importantly, MTV, which is based on relatively simple acquisition protocols, can be measured with very a high signal-to-noise ratio in feasible scan times (Abbas et al., 2014; Abbas et al., 2015; Volz et al., 2012). Thus, estimating MVF via MTV may provide an accurate and straightforward method to obtain a measure of the g-ratio. We term the MTV-based g-ratio-weighted MRI measurement  $GR^*$  since a portion of the variance in the signal might also reflect other tissue properties.

In the current study, we present the measurement of  $GR^*$  in the corpus callosum of 92 subjects, and evaluate changes in  $GR^*$  as a function of age and sex. Our results indicate first that the  $GR^*$  values obtained in the corpus callosum are similar to the g-ratio measured previously. Further findings are that  $GR^*$  is generally constant with age with no sex-related differences identified.

## 2. Methods

The current study utilized a large human database that was also used for our previous work (Yeatman et al., 2014) and (Gomez et al., 2017), as well as rodent data from West et al. (2016).

### 2.1. Human subjects

As previously reported, the Stanford University Institutional Review Board approved all data collection procedures and each adult participant provided informed consent, with the consent for each child participant provided by his parent/guardian. The participants in the study were healthy volunteers recruited from the San Francisco Bay Area based on information distributed in flyers, advertisements in local papers, and school newsletters. All participants were screened for neurological, psychiatric, and cognitive disorders. The age distribution of the sample purposefully included more subjects in the age bins that were expected to show the largest change in tissue properties, and fewer subjects in the age bins that were expected to have stable tissue properties. There were 29 participants aged 7–12, 12 participants aged 13–18, 9 participants aged 19–29, 10 participants aged 30–39, 7 participants aged 40–49, 8 participants aged 50–59, 8 participants aged 60–69, and 9 participants aged 70–85, giving a total of 92 participants (48 female participants). Four additional subjects were excluded due to registration error (see Section 2.3.3).

To estimate the reliability of the measurements, four additional adult subjects were re-scanned twice with the full protocol. For these subjects, the data required for MTV analysis were acquired a year apart, and the dMRI data several months apart. Data for these subjects were obtained at Stanford CNI, for details see (Gomez et al., 2017). In addition, four subjects were scanned with a modified dMRI protocol that allows an alternative modeling approach (Zhang et al., 2012) (see sections 2.2.2 and 2.3.2).

### 2.2. MRI acquisition and pre-processing

All human data were collected on a 3T General Electric Discovery 750 scanning system (General Electric Healthcare, Milwaukee, WI, USA) equipped with a 32-channel head coil (Nova Medical, Wilmington, MA, USA) at the Center for Cognitive and Neurobiological Imaging at Stanford University ([www.cni.stanford.edu](http://www.cni.stanford.edu)).

All animal data were acquired at Vanderbilt University on a 15.2T 11 cm horizontal bore Bruker (Rheinstetten, Germany) BioSpec scanner, using a 35 mm diameter Bruker quadrature volume coil for transmission and reception. For more information see (West et al., 2016).

### 2.2.1. MTV (and T1 and PD) mapping protocol

T1 relaxation was measured from spoiled gradient (SPGR) echo images acquired at different flip angles ( $\alpha = 4^\circ, 10^\circ, 20^\circ, 30^\circ$ , TR = 14 ms, TE = 2.4 ms). The scan resolution was 1 mm isotropic. The data contained an additional spin echo inversion recovery (SEIR) scan (Mezer et al., 2013). The SEIR was done with an echo planar imaging (EPI) read-out, a slab inversion pulse, and spectral spatial fat suppression. For the SEIR-EPI acquisition, the TR was 3 s; echo time was set to minimum full; inversion times were 50, 400, 1200, and 2400 ms. We used 2 mm<sup>2</sup> in-plane resolution with a slice thickness of 4 mm. The EPI read-out was performed using 2 × acceleration to minimize spatial distortions.

### 2.2.2. Diffusion MRI (dMRI)

dMRI data were acquired using twice-refocused spin echo diffusion-weighted sequences with full brain coverage. Diffusion weighting gradients were applied at 96 non-collinear directions across the surface of a sphere as determined by the electro-static repulsion algorithm (Jones et al., 1999). In all subjects, dMRI data were acquired at 2 mm isotropic spatial resolution and the diffusion weighting strength was set to  $b = 2000 \text{ s mm}^{-2}$  (TE/TR = 93.60/7800 ms, G = 53 mT/m,  $\delta = 21 \text{ ms}$ ,  $\Delta = 25.4 \text{ ms}$ ). We acquired eight non-diffusion-weighted  $b = 0$  images at the beginning of each measurement. A second, independent, dMRI data set was acquired on each subject using a low  $b$ -value ( $b = 1000 \text{ s mm}^{-2}$ ), 30-direction acquisition (TE/TR = 83.10/7100 ms,  $\delta = 17.6 \text{ ms}$ ,  $\Delta = 22 \text{ ms}$ ).

Additionally, four subjects (referred to below as S1–4) were scanned with an adjusted protocol that allows us to perform NODDI analysis (Zhang et al., 2012) (see below Section 2.3.2). For these subjects, the only differences in the acquisition were that both  $b$ -values were scanned with the same TE/TR (93.60/7800 ms), and the number of directions included in each shell. For  $b = 2000 \text{ s mm}^{-2}$ , 80 directions were used, and for  $b = 1000 \text{ s mm}^{-2}$ , 20 directions were used.

Subjects' motion was corrected using a rigid body alignment algorithm. Diffusion gradients were adjusted to account for the rotation applied to the measurements during motion correction. The twice-refocused spin echo sequence we used does not require eddy current correction (Reese et al., 2003). Preprocessing steps were implemented in MATLAB (MathWorks, Natwick, MI, USA) and are publicly available as part of the vistasoft git repository (<http://github.com/vistalab/vistasoft/mrDiffusion>; see dtiInit.m).

## 2.3. Metric computation

### 2.3.1. MTV

Whole-brain MTV maps were computed as described in Mezer et al. (2013) and Mezer et al. (2016); in short, unbiased T1 maps were calculated using the SPGRs which were corrected for B1 excite inhomogeneity using the unbiased SEIR data (Barral et al., 2010). The T1 maps were also used to calculate unbiased PD maps: To separate PD from receive-coil inhomogeneity, we assume smooth coil functions and use a biophysical regularization, which finds local linear relationships between  $1/T1$  and PD. This method was found to be effective and robust to noise (Mezer et al., 2016). The PD was normalized according to values in CSF-only voxels in the ventricles, to produce water-fraction (WF) maps. The MTV maps were then calculated as  $1-WF$ .

The analysis pipeline for producing unbiased T1, PD and MTV maps is an open-source MATLAB code (available at <https://github.com/mezera/mrQ>).

### 2.3.2. FVF

The diffusion data were fitted with a tensor model (Basser and Jones, 2002) from which the FA was derived. In this study, we used the  $b = 2000 \text{ s mm}^{-2}$  for all the analyses except for the calculations of the FA and FVF dependencies on  $b$ -value (Fig. 2). Previous work showed that the FA reflects both the dispersion and density of the fibers. However, in areas with high directional coherence (like the corpus callosum), the FVF

is a quadratic function (Eq. (1)) of FA (Stikov et al., 2011). Applying this function to our FA maps produced FVF maps in the corpus callosum.

$$FVF = 0.883FA^2 - 0.082FA + 0.074 \quad (1)$$

The diffusion data of subjects S1-4 (see above) were also analyzed using the NODDI toolbox (available at <http://mig.cs.ucl.ac.uk/index.php?n=Tutorial.NODDI matlab>) (Zhang et al., 2012). The NODDI model provides estimation of the fraction of three tissues compartment (Viso, the CSF volume fraction; Vic, the intra-cellular volume fraction; Vec, the extra-cellular volume fraction). Two NODDI parameters (Viso and Vic) were previously used to estimate AVF for  $g$ -ratio calculation (Cercignani et al., 2017; Stikov et al., 2015a). Specifically, the relevant expression is: Vic-(1-Viso). We compared the two diffusion components in the two  $g$ -ratio approaches, namely the tensor-based FVF and the NODDI derived expressions from the same subject's data.

### 2.3.3. GR\* Callosal maps

2.3.3.1. *GR\* computation.* The  $g$ -ratio can be calculated with MVF and FVF in Eq. (2) (Stikov et al., 2011).

$$g = \sqrt{1 - MVF/FVF} \quad (2)$$

FVF in the corpus callosum can be derived from diffusion data as described in 2.3.2. Here we can assume that  $MTV \approx MVF$  (Duval et al., 2017), in order to derive a weighted measurement of the  $g$ -ratio,  $GR^*$  (Eq. (3)).

$$GR^* = \sqrt{1 - MTV/FVF} \quad (3)$$

2.3.3.2. *T1 to b0-registration.* In order to combine the MTV and FVF to calculate the  $GR^*$  we must first co-register the quantitative MTV map of a subject to their dMRI data. The registration was computed to match the T1 map to the non-diffusion-weighted,  $b_0$  image as they have a relatively similar contrast. Next, we applied the calculated transformation to MTV map (since MTV and T1 are in the same imaging space), and resampled the MTV map to match the dMRI resolution. We used the ANTS software package (Avants et al., 2009) to calculate the transformation and to warp the MTV map. Manual inspection of the aligned images obtained after applying the diffeomorphic warp confirmed that the registration was accurate. The two volumes were compared using the mrView software (Tournier et al., 2012). Four subjects' data were excluded due to poor quality registration. An example of the registration quality in a single slice is shown in Supplementary Video 1.

Supplementary video related to this article can be found at <http://dx.doi.org/10.1016/j.neuroimage.2017.06.076>.

## 2.4. Corpus callosum segmentation

### 2.4.1. Tractography

Tractography was performed with a probabilistic algorithm, based on constrained spherical deconvolution, using the mrTrix software (Tournier et al., 2012). To avoid voxels with CSF partial volume, voxels around the ventricles with mean diffusivity (MD) greater than  $0.9 \text{ ms}/\mu\text{m}^2$  were excluded from the white matter mask on which the tractography was done. The white matter tracts were then segmented using the Automated Fiber Quantification (AFQ) toolbox (Yeatman et al., 2012). This software tracks the eight major callosal tracts connecting the two hemispheres: occipital, temporal, inferior-parietal, superior-parietal, motor, superior-frontal, anterior-frontal, and orbitofrontal (The toolbox is distributed at: <https://github.com/yeatmanlab/AFQ>).

### 2.4.2. Creating callosal sub-regions

Next, we used the tractography to create a voxelwise segmentation of the corpus callosum in each subject. We identified the mid-sagittal region of

each tract by intersecting the tract's projection with an inclusive corpus callosum ROI that was generated with mrDiffusion. This method produces overlapping sub-regions: since the streamlines are described in sub-voxel resolution (0.2 mm) AC-PC space, streamlines that were labeled as belonging to different tracts could pass through the same voxels. To control the overlap, each voxel was assigned a weight for each segment, reflecting the relative number of streamlines from that segment that pass through it. The code for the corpus callosum segmentation and voxel weights is released as open source in <https://github.com/shaiberman/mrGratio>.

**2.4.2.1. Minimizing the CSF contamination.** We assume CSF contamination is reflected in qMRI values. Particularly, contaminated corpus callosum voxels have high free water content and therefore higher T1 and MD than in typical white matter voxels. To minimize CSF contamination, voxels with MD greater than  $0.8 \text{ ms}/\mu\text{m}^2$  and T1 values greater than 1.1s were excluded from the analysis. Visually we find that this step removed mostly voxels bordering the ventricles.

## 2.5. Statistical comparisons

### 2.5.1. Comparison to other studies

**2.5.1.1. Agreement between MTV and histological MVF.** To validate our use of MTV as an estimate for MVF, we used the data published by West et al. (2016). A full description of the protocols can be found in West et al., and here we include a short description (see Supplementary Fig. 1 for a diagram). In their study, electron microscopy was used to quantify the myelin volume and it was compared to the qMRI MVF estimations. The analysis was done on different mouse models and in three callosal regions. The different animal models include three groups with conditional knockouts (CKO) and a control group. These groups were chosen since they display a wide range of myelin content. The models include mice with either a Tsc2 CKO (Carson et al., 2015), leading to extreme loss of myelin, a Rictor CKO (Carson et al., 2013), resulting in a less severe hypomyelination, or Pten CKO (Harrington et al., 2010), resulting in hypermyelination.

Electron microscopy estimates of myelin volume ( $MVF_{\text{hist}}$ ) were compared to two ex vivo qMRI measurements: multi-exponential T2 (Mackay et al., 1994) and quantitative MT (Gochberg and Gore, 2007). Additionally, West et al. estimated the water fraction using the multi-exponential T2 fit, where the sum of the T2 spectrum is the signal at  $TE = 0$ , or water proton density (Meyers et al., 2017; Whittall and MacKay, 1989). They normalized the water fraction of each brain to the value measured in cortical gray matter (GM) such that  $WF_{\text{West}} = WF/WF_{\text{GM}}$ .

Here, we further develop their calculation. We first re-calibrated the  $WF_{\text{West}}$  (water fraction normalized to gray matter) to obtain a value for the absolute water fraction. We reviewed the literature to find the appropriate scaling factor. Several sources estimated the water fraction of gray matter to be around 0.8–0.85 (see review in table 4.2, Tofts, 2005). In vivo studies in humans estimated the water fraction of gray matter to be around 0.833. In the data presented here we find the water fraction in gray matter to be 0.846, which is in good agreement with a number of other published values of 0.835, 0.815, and 0.833 (Abbas et al., 2014, 2015; Volz et al., 2012). Furthermore, West et al. (2016) calculated the theoretical WF of non-myelinated tissues (such as the mostly unmyelinated GM) and obtained a value of 0.859. We used the assumption that  $WF_{\text{GM}} \cong 0.859$  to calibrate West's original water fraction estimations. This provides us with the absolute ex vivo water fraction. We then calculated the fraction of no water, which we define as equivalent to  $MTV_{\text{ex vivo}}$  (Eq. (4)).

$$MTV_{\text{ex vivo}} = 1 - 0.859 \cdot WF_{\text{West}} \quad (4)$$

**2.5.1.2. Comparison to other histological g-ratio estimation.** To compare our measurements of  $GR^*$  with other reported findings, we used data from a study that used electron microscopy to directly measure the g-ratio along the corpus callosum of a single macaque monkey (Stikov et al., 2015a). Since in this study the corpus callosum was segmented anatomically (unlike the tractography based segmentation described here), we compared the values in the splenium, mid-body and genu of the corpus callosum, where the two segmentation methods have good agreement.

### 2.5.2. Sexual dimorphism of $GR^*$ with age

A permutation test was used to test for significant differences between the  $GR^*$  change of males and females with age. In each permutation, the data was randomly reassigned new sex labels and the  $GR^*$  of the group was fitted with a regression line. The slope difference between the groups was used to determine the p-value. To correct for the multiple (eight) comparisons, we set the threshold for statistical significance as 0.00125 (0.01/8). To test the effect of the chosen age range, we repeat this analysis for different age groups, varying the maximal age of the included subjects. This analysis was done only for age ranges with balanced male to female ratios.

To test for sexual dimorphism with age in MTV and FVF, we performed a similar test. For that purpose, each measurement's development with age was fitted with a model (for a discussion of our model of choice see Yeatman et al., 2014). A quadratic function was used for MTV, and an exponential function for FVF. The parameters of the model were then compared for sex differences.

## 3. Results

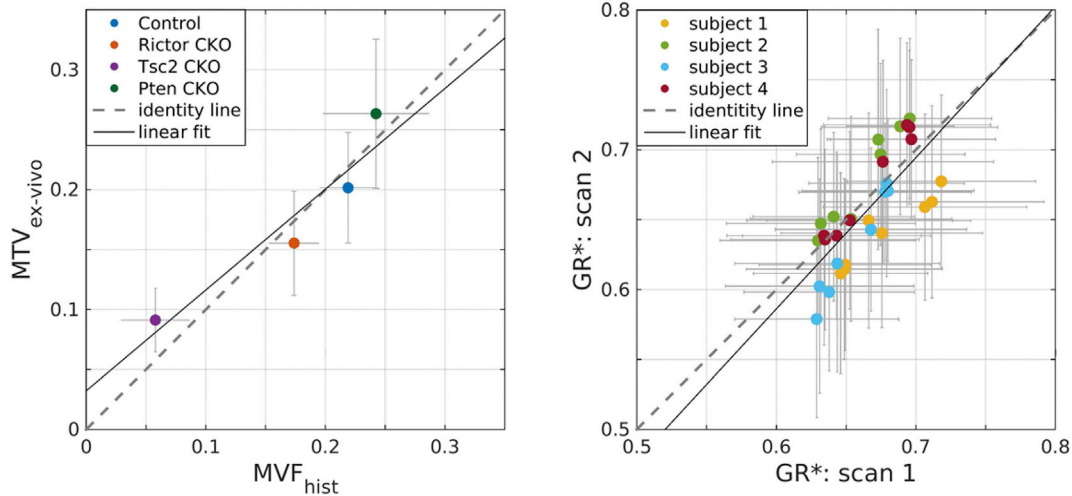
### 3.1. g-Ratio estimation across modalities

Fig. 1a shows the relationship between the histological measurement of the myelin volume fraction and the estimated MTV, derived from the multi-exponential T2 model. The high coefficient of determination ( $R^2 = 0.74$ ) is similar to the values found with more traditional myelin imaging methods (qMT,  $r = 0.84$ , and multi-exponential T2,  $r = 0.81$  (West et al., 2016)). Importantly, MTV estimations are unbiased by water exchange, while it has been shown to effect MWF and to a lesser extent qMT (Levesque and Pike, 2009; West et al., 2016). From this rodent data we calculated that the correlation coefficient between MTV and MVF as measured with qMT is 0.88 and with multi-exponential T2 0.78 (and 0.87 between qMT and multi-exponential T2).

In order to verify the reproducibility of our measurements, we evaluated the correlation between repeated scans for four subjects. The MTV data for these subjects were acquired a year apart, and the FVF data several months apart. We found that the values within each corpus callosum sub-region were highly reproducible ( $R^2 = 0.51$ ) (Fig. 1b).

Since the FVF estimation is based on FA, a parameter derived from the tensor model (Basser and Jones, 2002), we calculated the stability of FA and FVF as function of diffusion weighting b-value ( $1000 \text{ s mm}^{-2}$  compared with  $2000 \text{ s mm}^{-2}$ ) in the corpus callosum in all subjects. We found good stability across the two acquisitions for FA ( $R^2 = 0.74$ ) (Fig. 2 and therefore FVF ( $R^2 = 0.71$ ) (Supplementary Fig. 3).

We also tested whether the MTV-derived  $GR^*$  value in the corpus callosum is in agreement with previous MRI and non-MRI based g-ratio estimations. Fig. 3a shows the voxel-wise distribution of  $GR^*$  within the corpus callosum of all subjects. We found a range of  $GR^*$  values in the corpus callosum centered around a median of 0.69 (MAD = 0.05). These values are in agreement with ex vivo measures in rodents, where the reported results range from 0.6 to 0.8 (Arnett et al., 2001; Guy et al., 1989). In order to visualize the spatial distribution, the mean  $GR^*$  of the different callosal sub-regions were projected on the brain of a single subject (Fig. 3b). The results indicated a trend following the posterior-anterior axis, such that the  $GR^*$  was higher in the posterior segments of the corpus callosum. A one-way Anova test revealed a significant



**Fig. 1.  $GR^*$  model validation;** a.  $MTV_{ex-vivo}$ , the MRI-calculated non-water content, measured with T2 spectrum, as a function of the histological myelin volume fraction,  $MVF_{hist}$  (coefficient of determination,  $R^2 = 0.74$ ). Each data point represents a different mouse model of abnormal myelination, and an average over several animals and three regions along the corpus callosum. Data taken from West et al. (2016). b. The reproducibility of the human MRI-derived  $GR^*$  measurement, as the correlation between two separate scans ( $R^2 = 0.51$ ). The plot represents the mean  $GR^*$  ( $\pm$ std) of eight corpus callosum sub-regions from four subjects. The Bland-Altman plots of the same data are presented in Supplementary Fig. 2.

difference between the sub-regions ( $p < 0.001$ ).

We evaluated the  $GR^*$  along the corpus callosum, and compared our MTV-based estimations with values from other imaging studies, which used different qMRI parameters. Values reported in these studies include a mean g-ratio of 0.69 in human subjects (Mohammadi et al., 2015), 0.676, on a single macaque monkey (Stikov et al., 2015a,b), and 0.63 for five human subjects in vivo (Stikov et al., 2011). These experimental results are in agreement with the optimal g-ratio calculated analytically (0.6–0.77 (Chomiak and Hu, 2009; Rushton, 1951)). The relationship between the splenium, mid-body and genu regions of the corpus callosum agrees with histological findings: Fig. 3c shows the  $GR^*$  values, at the splenium, mid-body and genu regions of the corpus callosum, comparing our human data measurements to the g-ratio of a Macaque acquired with electron microscopy (published in (Stikov et al., 2015a)). Below the chart

is a representative image of the fibers crossing through the three sub-regions. In both the human and macaque, the mean g-ratio value in the splenium is significantly higher than in the more anterior segments of the corpus callosum. Furthermore, the same trend can be found in other human imaging studies, such as (Mohammadi et al., 2015).

### 3.2. Changes in $GR^*$ with age

Current theory predicts a small range of optimal g-ratio values. To test whether  $GR^*$  changes systematically with age, we evaluated  $GR^*$  in each corpus callosum sub-region as a function of age (6–80) (Fig. 4). Our results show that in most corpus callosum sub-regions  $GR^*$  there is little change with age. This is in contrast to the situation in the motor and anterior frontal sub-regions where there is a significant decrease or increase in  $GR^*$  with age ( $p < 0.001$ ), respectively.

The  $GR^*$  values are calculated from FVF derived from FA, and MTV. While both measurements change with age to some extent in the different corpus callosum sub regions (Supplementary Fig. 4 and 5), the FA values vary more than the MTV, and therefore FA drives the changes in  $GR^*$  to a greater extent. It therefore follows that the age-related changes in  $GR^*$  seen in the motor and anterior sub-regions can be attributed to alterations in FA and therefore FVF that are not fully accompanied by a change in MTV.

### 3.3. Investigation of $GR^*$ sexual dimorphism with age

Next, we tested the hypothesis suggesting sexual dimorphism during development affects the  $GR^*$ . Fig. 5 shows the  $GR^*$  as function of age for subjects younger than 50 years old ( $N = 67$ , 33 males). After correcting for multiple statistical comparisons, we found no significant differences between the change of  $GR^*$  with age in males versus females, in any of the callosal sub-regions. This is true irrespective of the choices of maximal age included in the analysis, including age ranges that better isolate development (p-values are presented in Supplementary Table 1). It is worth noting the presence of a small trend in our data, suggesting more sexual dimorphism in posterior segments of the corpus callosum. A similar test was used to test the presence of sexual dimorphism with age in FVF, and MTV, and no significant difference was found in any of the corpus callosum segments.

## 4. Discussion

Our analysis of 92 subjects demonstrates that MTV can be used

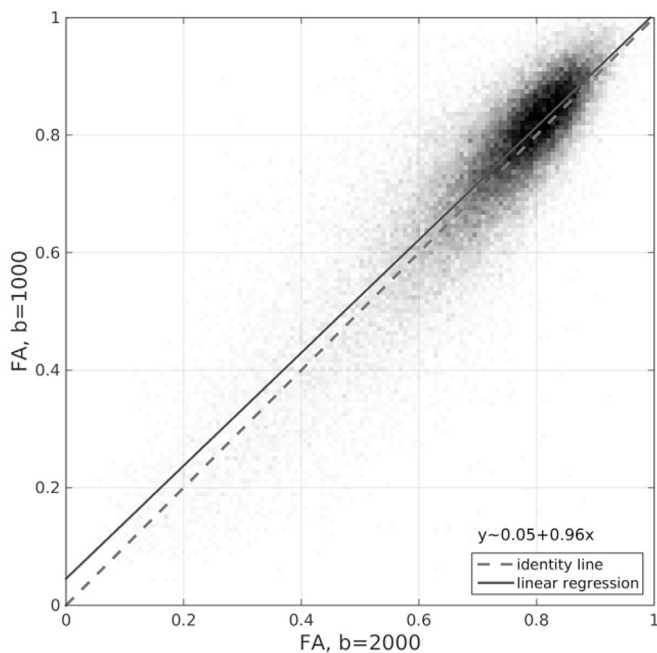


**Fig. 2. FA stability across b-values:** a 2D histogram of all of the FA values measured with two different diffusion weightings (b values in units of  $s\ mm^{-2}$ ). The values presented here are from the corpus callosum of all subjects ( $N = 92$ ). The agreement between FA of different diffusion weightings, quantified with the coefficient of determination, is high ( $R^2 = 0.74$ ).

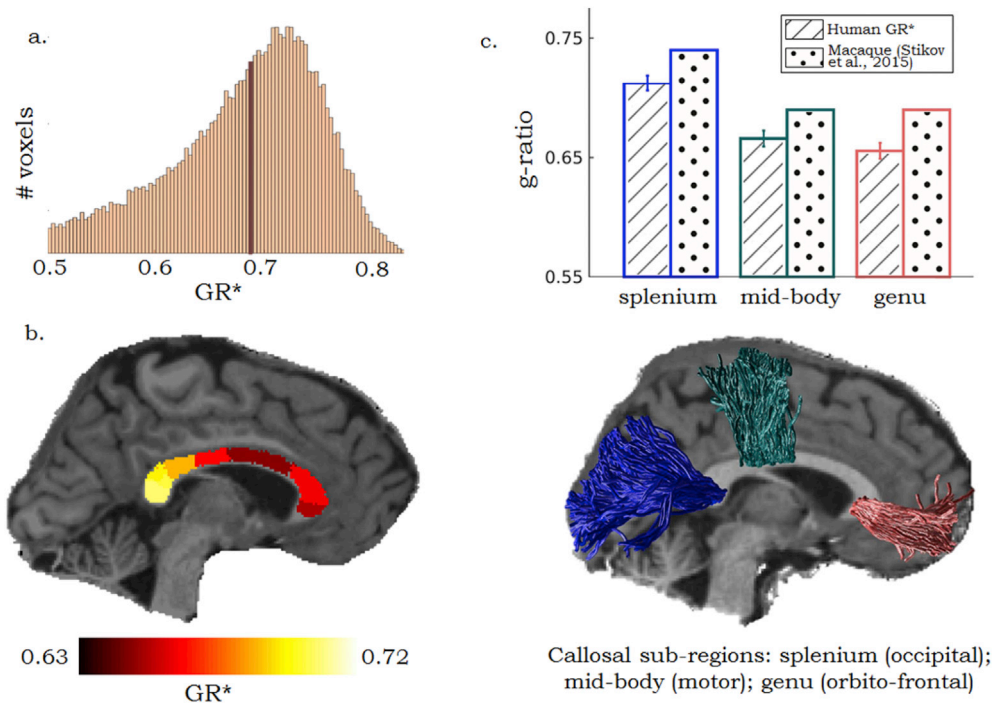


**Fig. 3. GR\* model vs. literature values:** a. histogram of GR\* values in the corpus callosum of all subjects, median GR\* = 0.69 (MAD = 0.05). b. Mean GR\* for each callosal sub-region in the test subjects, projected on the R1 map and callosal segmentation from a single subject. The value of GR\* changes as a function of callosal sub-region ( $p < 0.001$ ). c. Comparison of GR\* and histological g-ratio (from Stikov et al., 2015a) in the splenium, mid-body and genu regions, showing the anterior-posterior trend in these different areas. The image below the chart shows the fibers crossing through the sub-regions of the corpus callosum.

successfully to estimate the g-ratio in the corpus callosum in vivo. The results in Fig. 1 show that MTV represents a valid approximation of myelin volume to calculate GR\*. Fig. 3 shows the results are in agreement with the literature reports of ex vivo and in vivo measurements and also agree with theoretical calculations of optimal g-ratio values. Although in

two out of eight sub-regions in the corpus callosum we did detect a small but significant correlation with age, in the remaining six regions the value of GR\* remained constant with age (Fig. 4). In addition, we did not detect any significant sex-related differences in GR\* values with age (Fig. 5).

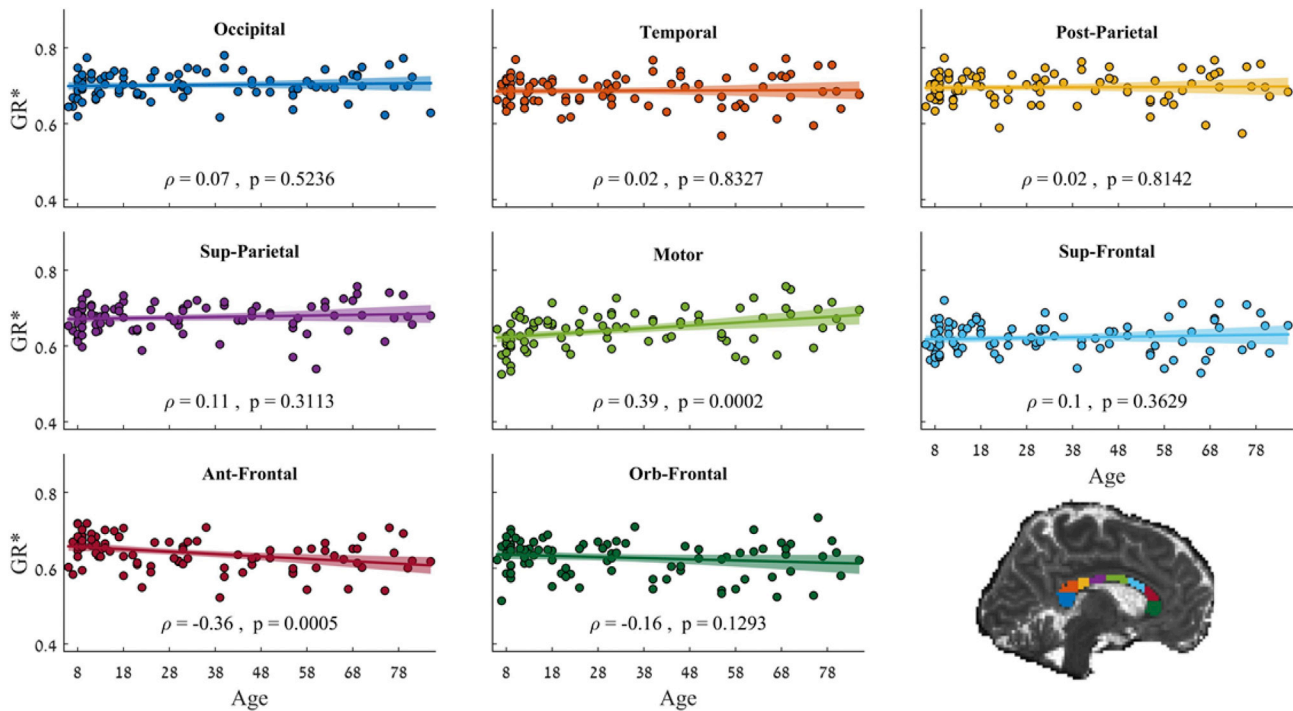


**Fig. 4. GR\* change with age.** Each subplot shows results for a different callosal sub-region (colors correspond to the arbitrary segmentation in the final image in the lower right panel). For each sub-region, the mean GR\* of the subjects is plotted as a function of age, as well as a regression line. In two of the eight sub-regions; the Motor Fiber crossing area and the Anterior Frontal crossing area, we found a significant correlation of GR\* with age. Each subplot notes the correlation coefficient ( $\rho$ ) and the corresponding p-value ( $p$ ).

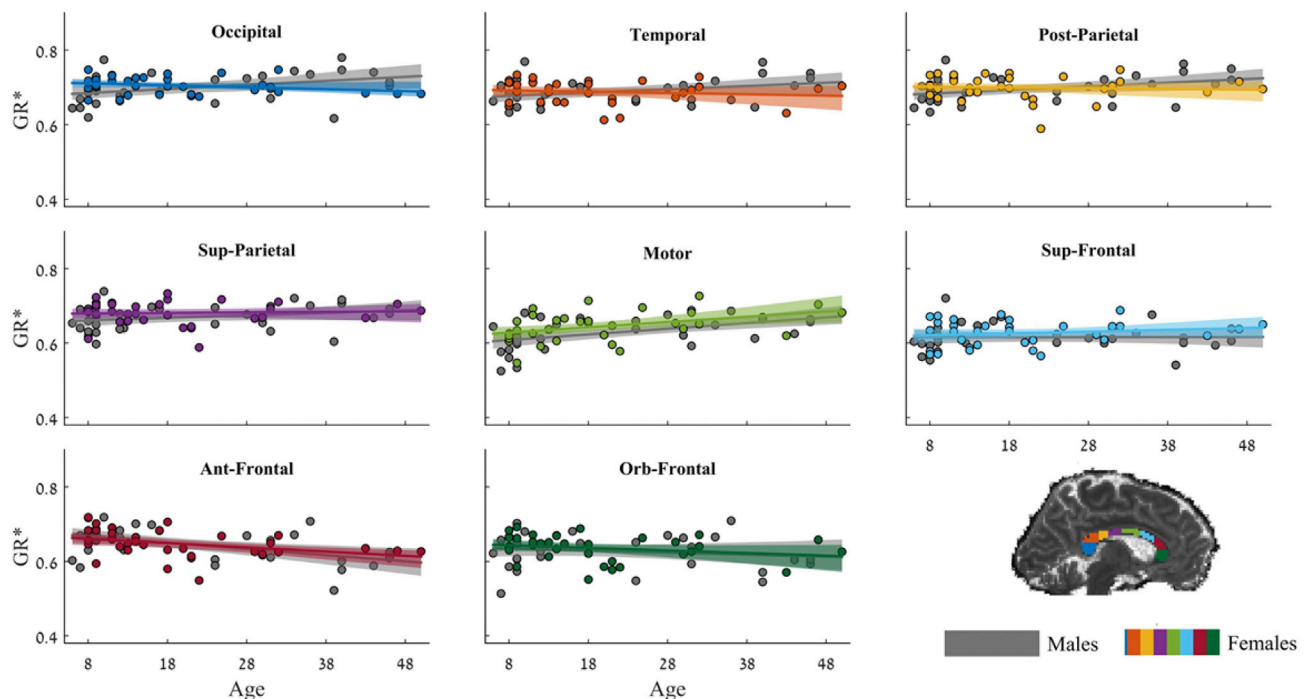


**Fig. 5.**  $GR^*$  changes with age and sex. Each subplot shows the results for a different callosal sub-region (color coded). For each sub-region, the mean  $GR^*$  of males and females of ages 8 to 50, is plotted as a function of age. In two of the eight sub-regions, the Motor and Anterior-Frontal regions, we found a significant correlation of  $GR^*$  with age. We found no significant differences (corrected for multiple comparisons) between the development of  $GR^*$  of males versus females, in any of the sub-regions.

Our observations that  $GR^*$  in the corpus callosum remains mostly stable across age and sex, agree with the theory that an optimal g-ratio can only exist within a relatively narrow range of values. The g-ratio is important for white matter efficiency and conduction fidelity (Chomiak and Hu, 2009; Rushton, 1951), and maintaining an optimal g-ratio is critical for reliable signal transduction in white matter. The need to remain within a narrow range of values may explain the overall stability of the  $GR^*$  while other quantitative tissue parameters (e.g., FA, T1, MD) do show changes with age (Bowley et al., 2010; Callaghan et al., 2014; Kochunov et al., 2012; Nagy et al., 2004; Voineskos et al., 2012; Yeatman et al., 2014).

Previous studies, specifically two human imaging studies, and one histological study on rodents, did detect a change in g-ratio with age. Using a qMT index to estimate MVF, and NODDI for AVF, Cercignani and colleagues found a slight increase in g-ratio in the forceps minor and forceps major of aging subjects. This apparent discrepancy with our data could be due to the different methods of estimating g-ratio together with the difference in dMRI modeling approaches (FA vs NODDI). Neither the MVF measurements presented here, nor those of the Cercignani study (estimated by MTV and qMT respectively) are specific to myelin and could be influenced by other tissue properties. While MTV is related to the total fraction of lipid and macromolecules, qMT is also sensitive to the specific types of lipid and macromolecules in the tissue (Kucharczyk et al., 1990). The MTV based estimation has the advantage that it does not involve multi-parameter model fitting, and does not rely on additional calibration.

The second in vivo study to measure a change in g-ratio with age (Dean et al., 2016), used much younger subjects, aged 3 months to 7.5 years of age. At that age the brain undergoes extensive development, which might affect the g-ratio to a greater extent than in older children and adults of the ages analyzed in our study.

The only histological study to measure g-ratio changes with age, observed a decrease in g-ratio in the optic nerve of aging mice (Stahon et al., 2016). The disagreement between this study and the human MRI results (both ours and those of Cercignani et al.) could be explained by various experimental differences: different species; a different white

matter pathway, different sensitivity and resolution of the analysis method (histology).

Our failure to detect any sexual dimorphism, replicates findings reported by Cercignani et al., but stands in contrast to an earlier hypothesis (Paus, 2010; Paus and Toro, 2009) based on a very large data set of qualitative measures in different brain regions (Paus and Toro, 2009). Recently, Pesaresi et al. reported a small but significant difference in the g-ratio in the splenium of young male and female rats, also supporting the sexual dimorphism hypothesis (Pesaresi et al., 2015). It is therefore possible that a small but significant difference may be present in humans in vivo and could be detected in a larger sample size of adolescent subjects. Alternatively, it is also possible that sexual dimorphism is a property of certain brain regions and is not manifested in the corpus callosum of humans. One explanation could be that the MRI derived g-ratio used here is not sensitive enough to detect the subtle changes measured histologically, at the level of individual axons.

Biomolecular studies, mostly in the peripheral nervous system, have demonstrated a correlation between axonal growth and myelination (de Waegh et al., 1992; Friede, 1972; Griffiths et al., 1998; Nave, 2010). Therefore, it is possible that while the changes reported in quantitative measurements in white matter do reflect changes in microstructure, in the corpus callosum these changes cancel out due to optimization mechanisms and leave the g-ratio relatively constant. Nevertheless, we did observe small but significant changes with age in  $GR^*$  in two callosal sub-regions. We find that most of these changes can be explained by the diffusion measurements. This implies a possible change in FVF that is not accompanied by changes in myelin. While changes in axonal caliber and myelination are often found to be correlated, as mentioned above, some evidence suggests that these processes may also occur independently (Edgar et al., 2004; Sánchez et al., 1996; Stevens et al., 2002). Alternatively, it possible that additional cellular mechanisms that are not accounted for in the  $GR^*$  model (e.g., change in glia content (Peters et al., 2000)) affect the diffusion and MTV signals to a different extent. These changes in  $GR^*$  are small and further research is needed in order to interpret the observations.

Finally, we also find a change in the  $GR^*$  as a function of callosum

sub-regions, such that higher values are found in posterior regions. This effect echoes similar results found via histology in the macaque (Stikov et al., 2015a) and with imaging (Mohammadi et al., 2015). Some of the effect found with MRI could be due to the different distribution of axons diameters in different regions in the corpus callosum, with more high-diameter axons ( $> 5\mu\text{m}$ ) found in the Splenium (Aboitiz et al., 1992; Farooq et al., 2016; Innocenti et al., 2015; Rabi et al., 2007). The general model used to calculate g-ratio with MRI was found to measure the aggregate g-ratio, and is therefore weighted more heavily by large axons, which in turn tend to have relatively less myelin (and therefore larger g-ratio) (Berthold et al., 1983). This could potentially affect the g-ratio weighted ( $\text{GR}^*$ ) results. Furthermore, a recent study showed changes along the corpus callosum in both DTI parameters as well as in MWF (Björnholm et al., 2017). In the current data the majority of the change in  $\text{GR}^*$  seems to originate from the FVF measurement (the variation of FVF and MTV along the corpus callosum can be seen in Supplementary Fig. 6). Our measurement, being derived from FA, is sensitive to the presence of other cellular compartments (e.g., Glia) (Beaulieu, 2002; Reyes-Haro et al., 2013) and dispersion in axon orientation. While there is no reason to assume higher dispersion in more posterior regions, especially given our comparison with the NODDI model (described below, and in Supplementary Fig. 8) which takes orientation into account, it has not been directly investigated to our knowledge, and cannot be ruled out.

#### 4.1. Limitations

MTV is the non-water fraction of a voxel that measures total lipid and macromolecular content. As such, in white matter it consists mainly (but not exclusively) of myelin. It was proposed, based on a review of the literature, that the non-myelin MTV roughly equals the water volume in myelin. This suggests that MTV measurements can be useful in approximating MVF in healthy tissue. It has been demonstrated that MTV is in good agreement with other qMRI myelin mapping techniques (qMT and MWF,  $r \cong 0.9$ ) (Mezer et al., 2013). Replicating this result, we find good correlation between the measurements ( $r > 0.78$ ), using ex vivo data from West et al. (2016). The MRI based MTV value range is very close to the volume of the myelin sheath (MVF) in white matter tissue estimated using histology: 25–30% (Mottershead et al., 2003; Perge et al., 2009; Stikov et al., 2015a,b). Our re-analysis of the results of West et al. shows a strong agreement ( $R^2 = 0.74$ ) between the histological MVF and MRI MTV estimations. Therefore, this approach seems to be at least comparable to the more elaborate qMRI approaches (qMT, MWF). Nevertheless, this assumption might not hold up in pathological situations, where the extra-axonal compartment is modified, or when the lipid and macromolecular content and organization changes. In some human pathology, unlike in the knockout models used in this paper, demyelination is often accompanied by significant infiltration of many other cells, that might lead to an increase in the macromolecular content, thus changing the relationship between MTV and MVF. Due to the strong observed dependency of MTV on myelin volume in healthy tissue (Fig. 1a), the assumption of  $\text{MTV} \cong \text{MVF}$  is acceptable when measuring  $\text{GR}^*$ , a g-ratio weighted in vivo measurement. A great benefit of the MTV-derived  $\text{GR}^*$  is the simple acquisition required (Abbas et al., 2014, 2015; Mezer et al., 2016; Volz et al., 2012). The  $\text{GR}^*$  could easily be measured on many existing databases, as well as on those being created currently.

In Fig. 1 we compare histological MVF and MTV (i.e., the non-water fraction) as calculated in West et al. In support of the  $\text{GR}^*$  model, we find good agreement between the two measurements. However, it is important to note that the MRI acquisition and analysis for the MTV measurement here is different from West et al., where they used multiple spin-echo, and fit a T2 exponential curve, such that the sum of the T2 spectrum is the signal at  $\text{TE} = 0$  (Whittall and MacKay, 1989). In humans, the MTV was derived by using variable flip-angle SPGR with a short TE ( $= 2$  ms). Furthermore, while our human data was collected in vivo on a 3T GE scanner, the data reported by West et al. was acquired post-

mortem from a fixated brain by employing a 15.2T BioSpec scanner with different signal-to-noise ratio. Nevertheless, while the acquisition methods are different, the final measurement of water content was previously validated for both approaches (i.e., for the SPGR protocol (Mezer et al., 2013) and for the T2 spectrum (Meyers et al., 2016)).

A last point is the estimation of FVF via dMRI parameters. In the current study, we chose to use FA as calculated with DTI. The relationship between FA and FVF was found in simulation and was not validated by histological data. Therefore, we cannot rule out other possible contributions to the FVF estimations. Furthermore, this FVF analysis is restricted only to the corpus callosum as it assumes coherent fiber orientation. On the other hand, alternative methods for measuring the FVF (and AVF) may require an additional dependency on the MVF estimate. This could cause any calibration error in the MVF to be propagated and have a dramatic effect on the g-ratio measurement (Campbell et al., 2017). One such method calculates FVF from parameters that are estimated using the NODDI model (Stikov et al., 2015a; Zhang et al., 2012), which is considered a more specific model of the tissue microstructure compared with the tensor model. A recent model suggested a mathematical model calculating simplified NODDI parameters from the tensor model (Edwards et al., 2017). Campbell et al. (2017) examined the correspondence between the FVF as derived from FA and the FVF derived from NODDI and found they are correlated, with NODDI-derived values in the corpus callosum consistently higher than FA-derived FVF. Performing the same comparison for four subjects, we find similar findings, showing a discrepancy between NODDI and FA derived FVF (Supplementary Fig. 7). The discrepancy could originate from the dependency of the NODDI-derived FVF on the MVF. Neither method is validated to date. Previous studies that use NODDI to calculate the g-ratio arrived at similar values to ours, either because of coarse normalization (Cercignani et al., 2017), or due to higher estimation of MVF (Stikov et al., 2015a,b). We performed an additional comparison between the FA derived FVF and the NODDI derived expression used to calculate FVF. In the corpus callosum of four subjects, where fiber orientation is highly coherent, these estimates are in agreement, suggesting they weigh similar structural properties of the tissue (Supplementary Fig. 8). This result is interesting considering the different interpretation of these measurements and further studies are needed to explain the differences in these formulations. Finally, we find FA-based FVF estimation to be stable across diffusion weighting, making it a reliable candidate for  $\text{GR}^*$  estimations. The independence of FA suggests that in future work FA could be averaged over the different b-values, potentially increasing SNR.

## 5. Conclusions

The MTV derived  $\text{GR}^*$  provides a simple and reliable in vivo estimation of the g-ratio in the human brain. It was used to test the stability of g-ratio with age and between the sexes. Unlike other tissue parameters measured with MRI,  $\text{GR}^*$  was shown to be mostly constant across a large age range. We therefore propose that these results support theoretical evidence suggesting that the g-ratio must remain within a narrow range of values around an optimal value for white matter function.

## Acknowledgements

We acknowledge R. Schurr for helpful advice and feedback. This work was supported ISF grant 0399306, awarded to A.A.M, by NSF/SBE-BSF (NSF no. 1551330 and BSF no. 2015608) awarded to A.A.M by Research on Schizophrenia and Depression (NARSAD) Young Investigator Grant from the Brain and Behavior Research Foundation awarded to A.A.M and J.D.Y, and NIH grant R01EB019980 awarded to M.D.D. We thank J. Gomez and K. Grill-Spector for providing data for testing reproducibility, their work was supported by NIH R01EY02988-A1. We also thank B. Wandell for data collection, which was supported by NSF/BCS-1228397 and NIH EY015000.

**Abbreviation list:**

|      |  |
|------|--|
| MVF  | myelin volume fraction                 |
| FVF  | fiber (axon + myelin) volume fraction  |
| AVF  | axon volume fraction                   |
| MTV  | lipid and macromolecular tissue volume |
| GR*  | g-ratio weighted measurement           |
| FA   | fractional anisotropy                  |
| MD   | mean diffusivity                       |
| CSF  | cerebrospinal fluid                    |
| WF   | water fraction                         |
| dMRI | diffusion MRI                          |
| qMRI | quantitative MRI                       |
| qMT  | quantitative magnetization transfer    |
| CKO  | conditional knockouts                  |

**Appendix A. Supplementary data**

Supplementary data related to this article can be found at <http://dx.doi.org/10.1016/j.neuroimage.2017.06.076>.

**References**

- Abbas, Z., Gras, V., Möllenhoff, K., Keil, F., Oros-Peusquens, A.M., Shah, N.J., 2014. Analysis of proton-density bias corrections based on T1 measurement for robust quantification of water content in the brain at 3 Tesla. *Magn. Reson. Med.* 72 (6), 1735–1745.
- Abbas, Z., Gras, V., Möllenhoff, K., Oros-Peusquens, A.M., Shah, N.J., 2015. Quantitative water content mapping at clinically relevant field strengths: a comparative study at 1.5T and 3T. *NeuroImage* 106, 404–413.
- Aboitiz, F., Scheibel, A.B., Fisher, R.S., Zaidel, E., 1992. Fiber composition of the human corpus callosum. *Brain Res.* 598 (1–2), 143–153.
- Albert, M., Antel, J., Brück, W., Stadelmann, C., 2007. Extensive cortical remyelination in patients with chronic multiple sclerosis. *Brain Pathol.* 17 (2), 129–138.
- Alexander, D.C., Hubbard, P.L., Hall, M.G., Moore, E.A., Ptito, M., Parker, G.J.M., Dyrby, T.B., 2010. Orientationally invariant indices of axon diameter and density from diffusion MRI. *NeuroImage* 52 (4), 1374–1389.
- Arnett, H., Mason, J., Marino, M., 2001. TNF $\alpha$  promotes proliferation of oligodendrocyte progenitors and remyelination. *Nat. Neurosci.* 4 (11), 1116–1122.
- Assaf, Y., Blumenfeld-Katzir, T., 2008. AxCaliber: a method for measuring axon diameter distribution from diffusion MRI. *Magn. Reson. Med.* 59 (6), 1347–1354.
- Avants, B., Tustison, N., Song, G., 2009. Advanced normalization tools (ANTS). *Insight J.* 2, 1–35.
- Barral, J.K., Gudmundson, E., Stikov, N., Etezadi-Amoli, M., Stoica, P., Nishimura, D.G., 2010. A robust methodology for in vivo T1 mapping. *Magn. Reson. Med.* 64 (4), 1057–1067.
- Basser, P.J., Jones, D.K., 2002. Diffusion-tensor MRI: theory, experimental design and data analysis - a technical review. *NMR Biomed.* 15 (7–8), 456–467.
- Beaulieu, C., 2002. The basis of anisotropic water diffusion in the nervous system - a technical review. *NMR Biomed.* 15 (7–8), 435–455.
- Berthold, C.-H., Nilsson, I., Rydmark, M., 1983. Axon diameter and myelin sheath thickness in nerve fibres of the ventral spinal root of the seventh lumbar nerve of the adult and developing cat. *J. Anat.* 136 (3), 483–508.
- Björholm, L., Nikkinen, J., Kiviniemi, V., Nordström, T., Niemelä, S., Drakesmith, M., et al., 2017. Structural properties of the human corpus callosum: multimodal assessment and sex differences. *NeuroImage* 152, 108–118.
- Bowley, M.P., Cabral, H., Rosene, D.L., Peters, A., 2010. Age changes in myelinated nerve fibers of the cingulate bundle and corpus callosum in the rhesus monkey. *J. Comp. Neurol.* 518 (15), 3046–3064.
- Callaghan, M.F., Freund, P., Draganski, B., Anderson, E., Cappelletti, M., Chowdhury, R., et al., 2014. Widespread age-related differences in the human brain microstructure revealed by quantitative magnetic resonance imaging. *Neurobiol. Aging* 35 (8), 1862–1872.
- Campbell, J.S.W., Leppert, I.R., Narayanan, S., Duval, T., Cohen-Adad, J., Pike, G.B., Stikov, N., 2017. Promise and pitfalls of g-ratio estimation with MRI. *arXiv Prepr. arXiv 1701.02760*.
- Carson, R.P., Fu, C., Winzenburger, P., Ess, K.C., 2013. Deletion of Rictor in neural progenitor cells reveals contributions of mTORC2 signaling to tuberous sclerosis complex. *Hum. Mol. Genet.* 22 (1), 140–152.
- Carson, R.P., Kelm, N.D., West, K.L., Does, M.D., Fu, C., Weaver, G., et al., 2015. Hypomyelination following deletion of Tsc2 in oligodendrocyte precursors. *Ann. Clin. Transl. Neurol.* 2 (12), 1041–1054.
- Cercignani, M., Giulietti, G., Dowell, N.G., Gabel, M., Broad, R., Leigh, P.N., et al., 2017. Characterizing axonal myelination within the healthy population: a tract-by-tract mapping of effects of age and gender on the fiber g-ratio. *Neurobiol. Aging* 49, 109–118.
- Chomiak, T., Hu, B., 2009. What is the optimal value of the g-ratio for myelinated fibers in the rat CNS? A theoretical approach. *PLoS One* 4 (11), e7754.
- Compston, A., Coles, A., 2008. Multiple sclerosis. *Lancet* 372 (9648), 1502–1517.
- Dean, D.C., O’Muircheartaigh, J., Dirks, H., Travers, B.G., Adluru, N., Alexander, A.L., Deoni, S.C.L., 2016. Mapping an index of the myelin g-ratio in infants using magnetic resonance imaging. *NeuroImage* 132, 225–237.
- de Waegh, S.M., Lee, V.M.-Y., Brady, S.T., 1992. Local modulation of neurofilament phosphorylation, axonal caliber, and slow axonal transport by myelinating Schwann cells. *Cell* 68 (3), 451–463.
- Deoni, S.C.L., Matthews, L., Kolind, S.H., 2013. One component? Two components? Three? the effect of including a nonexchanging “free” water component in multicomponent driven equilibrium single pulse observation of T1 and T2. *Magn. Reson. Med.* 70 (1), 147–154.
- Deoni, S.C.L., Rutt, B.K., Arun, T., Pierpaoli, C., Jones, D.K., 2008. Gleaning multicomponent T1 and T2 information from steady-state imaging data. *Magn. Reson. Med.* 60 (6), 1372–1387.
- Dula, A.N., Gochberg, D.F., Valentine, H.L., Valentine, W.M., Does, M.D., 2010. Multiexponential T2, magnetization transfer, and quantitative histology in white matter tracts of rat spinal cord. *Magn. Reson. Med.* 63 (4), 902–909.
- Duval, T., Lévy, S., Stikov, N., Campbell, J., Mezer, A., Witzel, T., et al., 2017. g-Ratio weighted imaging of the human spinal cord in vivo. *Neuroimage* 145, 11–23.
- Edgar, J.M., McLaughlin, M., Barrie, J.A., McCulloch, M.C., Garbern, J., Griffiths, I.R., 2004. Age-related axonal and myelin changes in the rumpshaker mutation of the P1p gene. *Acta Neuropathol.* 107 (4), 331–335.
- Edwards, L.J., Pine, K.J., Weiskopf, N., Mohammadi, S., 2017. NODDI-DTI: extracting neurite orientation and dispersion parameters from a diffusion tensor. *bioRxiv*. <http://dx.doi.org/10.1101/077099>.
- Ellerbrock, I., Mohammadi, S., 2016. Clinical usability of in vivo MR g-ratio mapping methods. In: 2016 Neuroscience Meeting Planner. Society for Neuroscience, San Diego, CA. Online.
- Farooq, H., Xu, J., Nam, J.W., Keefe, D.F., Yacoub, E., Georgiou, T., Lenglet, C., 2016. Microstructure imaging of crossing (MIX) white matter fibers from diffusion MRI. *Sci. Rep.* 6, 38927.
- Fields, R.D., 2008. White matter matters. *Sci. Am.* 298 (3), 42–49.
- Friede, R.L., 1972. Control of myelin formation by axon caliber. (With a model of the control mechanism). *J. Comp. Neurol.* 144 (2), 233–252.
- Gochberg, D.F., Gore, J.C., 2007. Quantitative magnetization transfer imaging via selective inversion recovery with short repetition times. *Magn. Reson. Med.* 57 (2), 437–441.
- Gomez, J., Barnett, M.A., Natu, V., Mezer, A., Palomero-Gallagher, N., Weiner, K.S., et al., 2017. Microstructural proliferation in human cortex is coupled with the development of face processing. *Science* 355 (6320), 68–71.
- Griffiths, I., Klugmann, M., Anderson, T., Yool, D., Thomson, C., Schwab, M.H., et al., 1998. Axonal swellings and degeneration in mice lacking the major proteolipid of myelin. *Science* 280 (5369), 1610–1613.
- Guy, J., Ellis, E.A., Kelley, K., Hope, G.M., 1989. Spectra of G ratio, myelin sheath thickness, and axon and fiber diameter in the Guinea pig optic nerve. *J. Comp. Neurol.* 287 (4), 446–454.
- Hampton, D.W., Innes, N., Merkler, D., Zhao, C., Franklin, R.J.M., Chandran, S., 2012. Focal immune-mediated white matter demyelination reveals an age-associated increase in axonal vulnerability and decreased remyelination efficiency. *Am. J. Pathol.* 180 (5), 1897–1905.

- Harrington, E.P., Zhao, C., Fancy, S.P.J., Kaing, S., Franklin, R.J.M., Rowitch, D.H., 2010. Oligodendrocyte PTEN is required for myelin and axonal integrity, not remyelination. *Ann. Neurol.* 68 (5), 703–716.
- Helms, G., Dathe, H., Kallenberg, K., Dechent, P., 2008. High-resolution maps of magnetization transfer with inherent correction for RF inhomogeneity and T1 relaxation obtained from 3D FLASH MRI. *Magn. Reson. Med.* 60 (6), 1396–1407.
- Innocenti, G.M., Carlen, M., Dyrby, T.B., 2015. The diameters of cortical axons and their relevance to neural computing. In: *Axons and Brain Architecture*, pp. 317–335.
- Jones, D.K., Horsfield, M.A., Simmons, A., 1999. Optimal strategies for measuring diffusion in anisotropic systems by magnetic resonance imaging. *Magn. Reson. Med.* 42 (3), 515–525.
- Kochunov, P., Williamson, D.E., Lancaster, J., Fox, P., Cornell, J., Blangero, J., Glahn, D.C., 2012. Fractional anisotropy of water diffusion in cerebral white matter across the lifespan. *Neurobiol. Aging* 33 (1), 9–20.
- Kucharczyk, W., Lenkinski, R.E., Kucharczyk, J., Henkelman, R.M., 1990. The effect of phospholipid vesicles on the NMR relaxation of water: an explanation for the MR appearance of the neurohypophysis? *AJNR. Am. J. Neuroradiol.* 11 (4), 693–700.
- Levesque, I.R., Pike, G.B., 2009. Characterizing healthy and diseased white matter using quantitative magnetization transfer and multicomponent T2 relaxometry: a unified view via a four-pool model. *Magn. Reson. Med.* 62 (6), 1487–1496.
- Mackay, A., Whittall, K., Adler, J., Li, D., Paty, D., Graeb, D., 1994. In vivo visualization of myelin water in brain by magnetic resonance. *Magn. Reson. Med.* 31 (6), 673–677.
- Meyers, S.M., Kollind, S.H., Laule, C., MacKay, A.L., 2016. Measuring water content using T2 relaxation at 3T: phantom validations and simulations. *Magn. Reson. Imaging* 34 (3), 246–251.
- Meyers, S.M., Kollind, S.H., MacKay, A.L., 2017. Simultaneous measurement of total water content and myelin water fraction in brain at 3T using a T2 relaxation based method. *Magn. Reson. Imaging* 37, 187–194.
- Mezer, A., Rokem, A., Berman, S., Hastie, T., Wandell, B.A., 2016. Evaluating quantitative proton-density-mapping methods. *Hum. Brain Mapp.* 37 (10), 3623–3635.
- Mezer, A., Yeatman, J.D., Stikov, N., Kay, K.N., Cho, N.-J., Dougherty, R.F., et al., 2013. Quantifying the local tissue volume and composition in individual brains with magnetic resonance imaging. *Nat. Med.* 19 (12), 1667–1672.
- Moeller, K., Willmes, K., Klein, E., 2015. A review on functional and structural brain connectivity in numerical cognition. *Front. Hum. Neurosci.* 9, 227.
- Mohammadi, S., Carey, D., Dick, F., Diedrichsen, J., Sereno, M.I., Reiser, M., et al., 2015. Whole-brain in-vivo measurements of the axonal g-ratio in a group of 37 healthy volunteers, 9, 441.
- Mottershead, J.P., Schmierer, K., Clemence, M., Thornton, J.S., Scaravilli, F., Barker, G.J., et al., 2003. High field MRI correlates of myelin content and axonal density in multiple sclerosis. *J. Neurol.* 250 (11), 1293–1301.
- Nagy, Z., Westerberg, H., Klingberg, T., 2004. Maturation of white matter is associated with the development of cognitive functions during childhood. *J. Cogn. Neurosci.* 16, 1227–1233.
- Nave, K.-A., 2010. Myelination and support of axonal integrity by glia. *Nature* 468 (7321), 244–252.
- Paus, T., 2010. Growth of white matter in the adolescent brain: myelin or axon? *Brain Cogn.* 72 (1), 26–35.
- Paus, T., Toro, R., 2009. Could sex differences in white matter be explained by g ratio? *Front. Neuroanat.* 3, 14.
- Perge, J.A., Koch, K., Miller, R., Sterling, P., Balasubramanian, V., 2009. How the optic nerve allocates space, energy capacity, and information. *J. Neurosci. Off. J. Soc. Neurosci.* 29 (24), 7917–7928.
- Pesaresi, M., Soon-Shiong, R., French, L., Kaplan, D.R., Miller, F.D., Paus, T., 2015. Axon diameter and axonal transport: in vivo and in vitro effects of androgens. *NeuroImage* 115, 191–201.
- Peters, A., Moss, M.B., Sethares, C., 2000. Effects of aging on myelinated nerve fibers in monkey primary visual cortex. *J. Comp. Neurol.* 419 (3), 364–376.
- Rabi, S., Madhavi, C., Antonisamy, B., Koshi, R., 2007. Quantitative analysis of the human corpus callosum under light microscopy. *Eur. J. Anat.* 11 (2), 95.
- Reese, T.G., Heid, O., Weisskoff, R.M., Wedeen, V.J., 2003. Reduction of eddy-current-induced distortion in diffusion MRI using a twice-refocused spin echo. *Magn. Reson. Med.* 49 (1), 177–182.
- Reisert, M., Mader, I., Umarova, R., Maier, S., Tebartz van Elst, L., Kiselev, V.G., 2013. Fiber density estimation from single q-shell diffusion imaging by tensor divergence. *NeuroImage* 77, 166–176.
- Reyes-Haro, D., Mora-Loyola, E., Soria-Ortiz, B., García-Colunga, J., 2013. Regional density of glial cells in the rat corpus callosum. *Biol. Res.* 46 (1), 27–32.
- Rushton, W.A.H., 1951. A theory of the effects of fibre size in medullated nerve. *J. Physiol.* 115 (1), 10.
- Sánchez, I., Hassinger, L., Paskevich, P.A., Shine, H.D., Nixon, R.A., 1996. Oligodendroglia regulate the regional expansion of axon caliber and local accumulation of neurofilaments during development independently of myelin formation. *J. Neurosci. Off. J. Soc. Neurosci.* 16 (16), 5095–5105.
- Sled, J.G., Pike, G.B., 2001. Quantitative imaging of magnetization transfer exchange and relaxation properties in vivo using MRI. *Magn. Reson. Med.* 46 (5), 923–931.
- Stahon, K.E., Bastian, C., Griffith, S., Kidd, G.J., Brunet, S., Baltan, S., 2016. Age-related changes in axonal and mitochondrial ultrastructure and function in white matter. *J. Neurosci.* 36 (39), 9990–10001.
- Stevens, B., Porta, S., Haak, L.L., Gallo, V., Fields, R.D., 2002. Adenosine: a neuron-glial transmitter promoting myelination in the CNS in response to action potentials. *Neuron* 36 (5), 855–868.
- Stikov, N., Campbell, J.S.W., Stroh, T., Lavelée, M., Frey, S., Novek, J., et al., 2015a. In vivo histology of the myelin g-ratio with magnetic resonance imaging. *NeuroImage* 118, 397–405.
- Stikov, N., Campbell, J.S.W., Stroh, T., Lavelée, M., Frey, S., Novek, J., et al., 2015b. Data in Brief Quantitative analysis of the myelin g-ratio from electron microscopy images of the macaque corpus callosum. *Data Brief* 4, 368–373.
- Stikov, N., Perry, M.L., Mezer, A., Rykhlevskaia, E., Wandell, B.A., Pauly, J.M., Dougherty, R.F., 2011. Bound pool fractions complement diffusion measures to describe white matter micro and macrostructure. *NeuroImage* 54 (2), 1112–1121. <http://www.sciencedirect.com/science/article/pii/S1053811910011651>.
- Tofts, P. (Ed.), 2005. *Quantitative MRI of the Brain: Measuring Changes Caused by Disease*. John Wiley & Sons.
- Tournier, J.-D., Calamante, F., Connelly, A., 2012. MRtrix: diffusion tractography in crossing fiber regions. *Int. J. Imaging Syst. Technol.* 22 (1), 53–66.
- Voineskos, A.N., Rajji, T.K., Lobaugh, N.J., Miranda, D., Shenton, M.E., Kennedy, J.L., et al., 2012. Age-related decline in white matter tract integrity and cognitive performance: a DTI tractography and structural equation modeling study. *Neurobiol. Aging* 33 (1), 21–34.
- Volz, S., Nöth, U., Deichmann, R., 2012. Correction of systematic errors in quantitative proton density mapping. *Magn. Reson. Med.* 68 (1), 74–85.
- West, K.L., Kelm, N.D., Carson, R.P., Does, M.D., 2015. A revised model for estimating g-ratio from MRI. *NeuroImage* 125, 1155–1158.
- West, K.L., Kelm, N.D., Carson, R.P., Gochberg, D.F., Ess, K.C., Does, M.D., 2016. Myelin volume fraction imaging with MRI. *NeuroImage*. <http://www.sciencedirect.com/science/article/pii/S1053811916307935>.
- Whittall, K.P., MacKay, A.L., 1989. Quantitative interpretation of NMR relaxation data. *J. Magn. Reson.* (1969) 84 (1), 134–152.
- Wolswijk, G., 2002. Oligodendrocyte precursor cells in the demyelinated multiple sclerosis spinal cord. *Brain* 125 (2), 338–349.
- Yarnykh, V.L., 2007. Actual flip-angle imaging in the pulsed steady state: a method for rapid three-dimensional mapping of the transmitted radiofrequency field. *Magn. Reson. Med.* 57 (1), 192–200.
- Yeatman, J.D., Dougherty, R.F., Myall, N.J., Wandell, B.A., Feldman, H.M., 2012. Tract profiles of white matter properties: automating fiber-tract quantification. *PLoS One* 7 (11).
- Yeatman, J.D., Dougherty, R.F., Rykhlevskaia, E., Sherbondy, A.J., Deutsch, G.K., Wandell, B.A., Ben-Shachar, M., 2011. Anatomical properties of the arcuate fasciculus predict phonological and reading skills in children. *J. Cogn. Neurosci.* 23 (11), 3304–3317.
- Yeatman, J.D., Wandell, B.A., Mezer, A.A., 2014. Lifespan maturation and degeneration of human brain white matter. *Nat. Commun.* 5, 4932.
- Zatorre, R.J., Fields, R.D., Johansen-Berg, H., 2012. Plasticity in gray and white: neuroimaging changes in brain structure during learning. *Nat. Neurosci.* 15 (4), 528–536.
- Zhang, H., Schneider, T., Wheeler-Kingshott, C.A., Alexander, D.C., 2012. NODDI: practical in vivo neurite orientation dispersion and density imaging of the human brain. *NeuroImage* 61 (4), 1000–1016.